XIII International Conference on Computational Plasticity. Fundamentals and Applications
COMPLAS XIII
E. Oñate, D.R.J. Owen, D. Peric & M. Chiumenti (Eds)

EFFICIENT COMPUTATIONAL HOMOGENIZATION OF SIMPLE ELASTO-PLASTIC MICROSTRUCTURES USING A MODIFIED RITZ-GALERKIN APPROACH

Stephan Wulfinghoff*, Stefanie Reese*

*Institute of Applied Mechanics, RWTH Aachen University
Mies-van-der-Rohe-Str. 1, 52074 Aachen, Germany
e-mail: {stephan.wulfinghoff, stefanie.reese}@ifam.rwth-aachen.de, web page: www.ifam.rwth-aachen.de

Key words: Computational Homogenization, Plasticity, Microstructures, Ritz-Galerkin

Abstract. In this presentation, a recent work [18] on a fast nonlinear homogenization method for simple microstructures is revised. The degrees of freedom of the approach are defined on shear bands. Moreover, the number of degrees of freedom as well as the number of stress computations is very small compared to related finite element (FE) computations making the method fast. The predictions of the computational method are validated by FE-simulations. As a new aspect, the overall algorithmic tangent moduli of the method are derived for the first time.

1 INTRODUCTION

Composite materials and materials with well-defined microstructure have good mechanical properties and a relatively small weight, which makes them attractive for many industrial applications. Moreover by design of their microstructure their mechanical properties of engineering components can be adjusted individually and adapted to the application at hand. In this context, homogenization represents a well suited engineering tool to predict the macroscopic mechanical behavior based on the geometry of the microstructure and the material properties of the individual phases. Early homogenization schemes [10, 13] have been further developed based on findings of Eshelby [2] which led to several well-known homogenization schemes, like that of Mori and Tanaka [8] or the self-consistent scheme (e.g. [6]). In the case of linear material behavior analytical homogenization methods usually provide fast and sufficiently accurate predictions. However, in the non-linear case more advanced computational homogenization methods are usually applied, like the FE-method [3]. This is even more complex if size-effects must be taken into account in an efficient manner [14–17]. Computational non-linear homogenization represents a very accurate method. However, it can usually not be applied in real two scales simulations due

to the high computational effort. Therefore, several authors proposed faster approaches in order to homogenize non-linear material behavior. In this context Moulinec and Suquet [9] proposed a very fast method based on the fast Fourier transform algorithm, which is nowadays used by many authors ([12], [5], amongst many others). In addition, the transformation field analysis, which has been proposed by Dvorak [1], is used by many authors as well as the nonuniform transformation field analysis (NTFA), which was proposed by Michel and Suquet [7] (see, e.g., [4]). In particular, if large deformations are considered proper orthogonal decomposition based methods are often applied. A method to increase their efficiency is discussed by Ryckelynck [11]. This type of method is not restricted to periodic problems like for example the FFT method.

Notation. A direct tensor notation is preferred throughout the text. Vectors and 2nd-order tensors are denoted by bold letters, e. g. $\boldsymbol{a}$ or $\boldsymbol{A}$. The symmetric part of a 2nd-order tensor $\boldsymbol{A}$ is designated by $\mathrm{sym}(\boldsymbol{A})$. A linear mapping of 2nd-order tensors by a 4th-order tensor is written as $\boldsymbol{A} = \boldsymbol{C}[\boldsymbol{B}]$. The scalar product and the dyadic product of 2nd-order tensors are denoted, e. g. by $\boldsymbol{A} \cdot \boldsymbol{B} = \mathrm{tr}(\boldsymbol{A}^{\mathsf{T}}\boldsymbol{B})$ and $\boldsymbol{A} \otimes \boldsymbol{B}$, respectively.

2 DESCRIPTION OF THE PROPOSED METHOD

The aim of the presentation is to give a summary of a recent work [18] on an efficient homogenization method for physically non-linear material behavior, which is particularly suited for materials with hard elastic inclusions and a soft inelastic matrix. Here, the inelastic matrix strains are assumed to be incompressible or nearly incompressible. The methods may also work for compressible inelastic matrix deformations, but this case is not within the scope of this work. Specifically, plastic matrix deformations are considered. A typical deformation mechanism in the aforementioned type of microstructure is given by shear bands. Within a periodic representative volume element (RVE) these shear bands usually have preferred directions, for example horizontal, vertical or diagonal.

In many cases, the principle deformation mechanism within a shear band is given by a simple shear. Often a deformation triggers a strongly localized strain in several shear bands, the superposition of which leads to a deformation pattern, which is sometimes complex such that the individual shear bands are hardly recognizable. In this work, the deformation within a periodic RVE with simple geometry is idealized in form of an average strain with superposed shear bands. The degrees of freedom are given by the shear and normal deformations in the individual shear bands.

The method may be applied to materials with heterogeneous microstructure like composite materials or, e.g., dual-phase steels with martensitic inclusions.

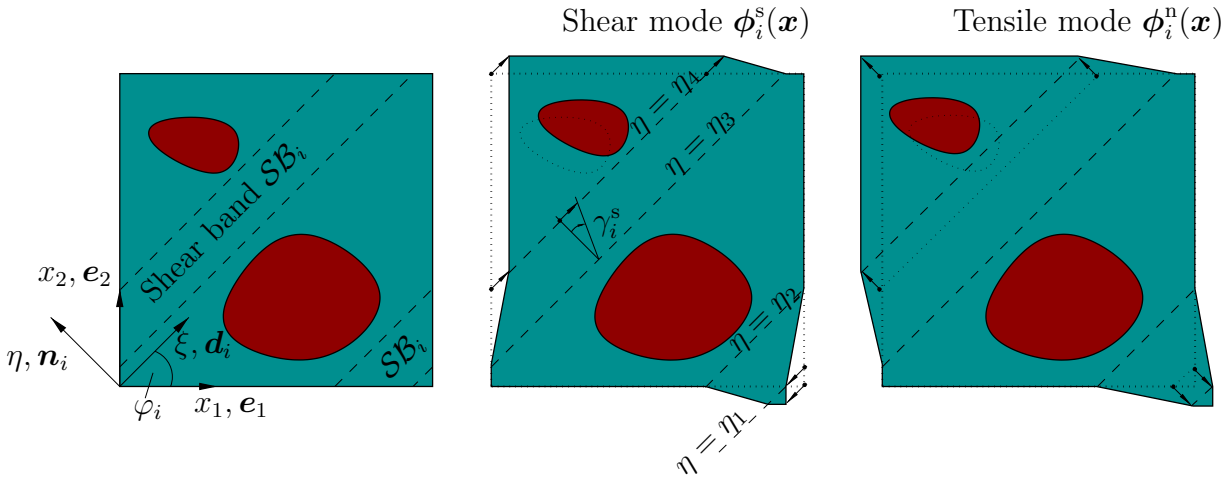

Figure 1: Shear band $\mathcal{SB}_i$ (left) and shape-functions of the shear $\boldsymbol{\phi}_i^{\mathrm{s}}(\boldsymbol{x})$ (center) and tensile modes $\boldsymbol{\phi}_i^{\mathrm{n}}(\boldsymbol{x})$ (right). The set $\mathcal{SB}_i$ represents the points in the shear band.

3 DISCRETIZATION

A usual Ritz-Galerkin approach is used, which means that the displacement is given by

$$\boldsymbol{u}(\boldsymbol{x},t) = \boldsymbol{\varepsilon}_0(t)\boldsymbol{x} + \sum_{i=1}^{N} \gamma_i^{\mathrm{s}}(t)\boldsymbol{\phi}_i^{\mathrm{s}}(\boldsymbol{x}) + \sum_{i=1}^{N} \gamma_i^{\mathrm{n}}(t)\boldsymbol{\phi}_i^{\mathrm{n}}(\boldsymbol{x}). \tag{1}$$

Here, $\boldsymbol{u}(\boldsymbol{x},t)$ denotes the displacement field. The $\boldsymbol{\phi}_i^{\mathrm{s}}(\boldsymbol{x})$ and $\boldsymbol{\phi}_i^{\mathrm{n}}(\boldsymbol{x})$ represent $2N$ ansatz functions. In addition, γ_i^{s} and γ_i^{n} denote the associated degrees of freedom. The strain $\varepsilon = 0$ will be discussed subsequently. The ansatz functions $\boldsymbol{\phi}_i^{\mathrm{s}}(\boldsymbol{x})$ and $\boldsymbol{\phi}_i^{\mathrm{n}}(\boldsymbol{x})$ represent shear modes and normal modes, which are defined on the N shear bands. Each shear band represents a set of points and is denoted by $\mathcal{SB}_i$. Here, i is the shear band index. The same ansatz functions as in [18] are used. As a result, the strain is given by

$$\boldsymbol{\varepsilon} = \mathrm{sym}(\nabla \boldsymbol{u}) = \boldsymbol{\varepsilon}_0 + \sum_i I_i(\boldsymbol{x})(\gamma_i^{\mathrm{s}}\boldsymbol{M}_i^{\mathrm{s}} + \gamma_i^{\mathrm{n}}\boldsymbol{M}_i^{\mathrm{n}}). \tag{2}$$

Here, $\boldsymbol{M}_i^{\mathrm{s}} = \mathrm{sym}(\boldsymbol{d}_i \otimes \boldsymbol{n}_i)$ and $\boldsymbol{M}_i^{\mathrm{n}} = \boldsymbol{n}_i \otimes \boldsymbol{n}_i$ denote shear and normal strain modes. The vectors $\boldsymbol{d}_i$ and $\boldsymbol{n}_i$ are unit vectors in the direction of the shear band and perpendicular, respectively. They are illustrated in Fig. 1. In Eq. (2), the function $I_i(\boldsymbol{x})$ represents the usual indicator function.

The introduction of several shear bands implies different regions r^j. In each of these regions the strain is constant. This means that the stresses must be computed in all regions (see Fig. 2). Upper indices are related to regions in the following.

The strain tensor $\boldsymbol{\varepsilon}_0$ can be shown to be given by

$$\boldsymbol{\varepsilon}_0 = \boldsymbol{\varepsilon}_0(\bar{\boldsymbol{\varepsilon}}, \hat{\gamma}) = \bar{\boldsymbol{\varepsilon}} - \sum_i c_i(\gamma_i^{\mathrm{s}}\boldsymbol{M}_i^{\mathrm{s}} + \gamma_i^{\mathrm{n}}\boldsymbol{M}_i^{\mathrm{n}}) \tag{3}$$

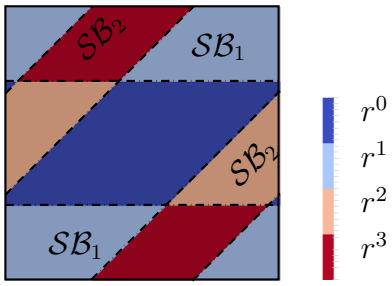

Figure 2: Regions r^j. The strains inside of the regions $\boldsymbol{\varepsilon}^j(t)$ are homogeneous [18].

with $\hat{\gamma} = (\gamma_1^{\mathrm{s}}, \dots, \gamma_N^{\mathrm{s}}, \gamma_1^{\mathrm{n}}, \dots \gamma_N^{\mathrm{n}})$.
Assuming a quasi-static situation and neglecting body forces the equilibrium conditions can be given in weak form by

$$\int_\Omega \boldsymbol{\sigma} \cdot \delta\boldsymbol{\varepsilon} \, \mathrm{d}\Omega = 0. \tag{4}$$

With Eq. (2), the equilibrium condition yields the following residual for the normal modes:

$$\tilde{\sigma}_i = c_i \boldsymbol{M}_i^{\mathrm{n}} \cdot (\bar{\boldsymbol{\sigma}}_i - \bar{\boldsymbol{\sigma}}) = 0. \tag{5}$$

Here, c_i represent the volume fractions of the shear bands, $\bar{\boldsymbol{\sigma}}_i$ is the average stress in shear band $\mathcal{SB}_i$ and $\bar{\boldsymbol{\sigma}}$ is the average stress of the total volume Ω. Similar expressions can be derived for the shear modes. In total, the residual vector can be written as

$$\hat{\sigma} = (\tilde{\tau}_1, \dots, \tilde{\tau}_N, \tilde{\sigma}_1, \dots, \tilde{\sigma}_N) = \hat{0}. \tag{6}$$

The unknowns of this non-linear system of equations are given by $\hat{\gamma} = (\gamma_1^{\mathrm{s}}, \dots, \gamma_N^{\mathrm{s}}, \gamma_1^{\mathrm{n}}, \dots \gamma_N^{\mathrm{n}})$. This system of non-linear equations must be linearized in order to be solved by a conventional Newton scheme. The computation of the stresses requires the evaluation of the material subroutine in each region r^j. Therefore, standard subroutines can be used, which are usually applied at the integration points of conventional finite element simulations. In addition, the consistent tangent operators are needed in order to compute the stiffness matrix related to Eq. (6) (for further details see [18]). It should be noted that usually, a small number of degrees of freedom is sufficient if the geometry of the microstructure is simple (for example two inclusions). Therefore, the numerical effort to solve the arising linear systems of equations is significantly smaller than in a conventional finite element simulation of comparable microstructures. Moreover, the assembly procedure of the stiffness matrix requires a significantly smaller number of material subroutine calls than in an FE-computation, where the number of integration points is much larger than the number of regions at hand. This allows to compute the average stress significantly faster than in an FE-computation.

4 MODIFICATION OF THE MODEL

The application of the Ritz-Galerkin scheme usually leads to a mechanical response, which is too stiff. Therefore, two modifications are proposed in order to reduce the stiffness of the discretized model. As a first modification (Modification I) the volume fraction of the hard-elastic inclusions inside of the shear bands is artificially reduced. A parameter $\alpha \in [0,1]$ allows to vary the stiffness of the shear bands. In this context, $\alpha = 0$ means that the volume fractions of the inclusions inside of the shear bands are not altered, hence an overprediction of the stiffness can be expected. In contrast, $\alpha = 1$ means that all inclusion material is replaced by the material of the matrix inside of the shear bands.

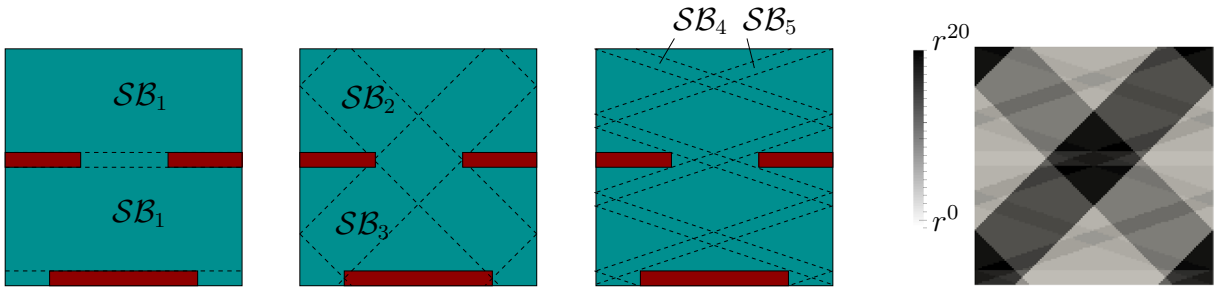

Figure 3: First three pictures: shear bands $\mathcal{SB}_1$ to $\mathcal{SB}_5$. Right picture: the intersection of the shear bands leads to 21 regions $r^0, ..., r^{20}$. In these regions, $\boldsymbol{\varepsilon}^0, ..., \boldsymbol{\varepsilon}^{20}$ are homogeneous [18].

The second modification (Modification II) is based on a volumetric-deviatoric decoupling of the strain. The stress response to the volumetric strain is assumed to be elastic. The associated elastic constants are determined by a finite element simulation with a small prescribed volumetric strain. This is standard in RVE computations. Moreover, the stress response to the strain deviator is computed using the shear band model. This means that the prescribed strain for the shear band model is given by $\bar{\boldsymbol{\varepsilon}}'(t) = \bar{\boldsymbol{\varepsilon}}(t) - \bar{\boldsymbol{\varepsilon}}^\circ(t)$. Here, $\bar{\boldsymbol{\varepsilon}}^\circ$ represents the spherical part of the strain tensor, whereas $\bar{\boldsymbol{\varepsilon}}'$ is the strain deviator. In summary, the stress is computed by the formula

$$\bar{\boldsymbol{\sigma}} = \mathbb{K}[\bar{\boldsymbol{\varepsilon}}^\circ] + \bar{\boldsymbol{\sigma}}_{\mathrm{SB}}. \tag{7}$$

This modification is motivated as follows. If the prescribed strain is a purely spherical tensor, which is applied to the shear band model, and both materials (inclusion and matrix material) are isotropic, then the result is equal to that of the classical Voigt homogenization scheme, which is known to yield results, which are significantly to stiff if the phase contrast is large.

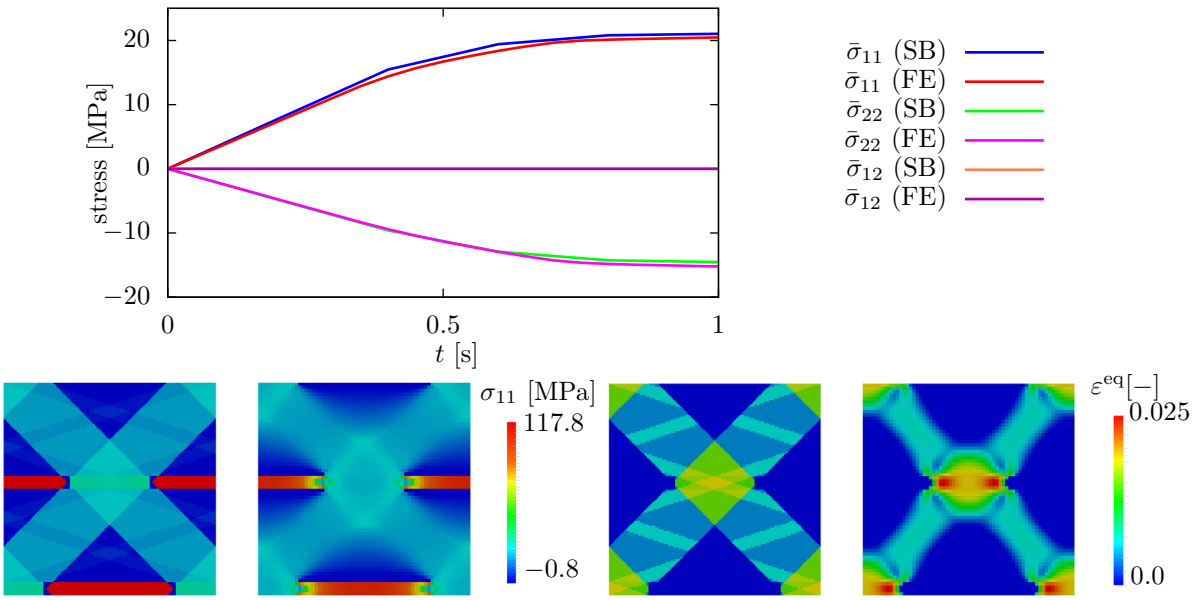

Figure 4: Diagram: Average stress curves of shear band approach (SB) FE-model (FE). The prescribed average strain is given by $\bar{\boldsymbol{\varepsilon}}(t) = \dot{\varepsilon}_0 t(\boldsymbol{e}_1 \otimes \boldsymbol{e}_1 - \boldsymbol{e}_2 \otimes \boldsymbol{e}_2)$. Other figures: FE-results and shear band solution. The regions of the fibres that were replaced by matrix material (Modification I) are colored in blue (Figure taken from [18]).

5 ALGORITHMIC TANGENT

The overall algorithmic tangent may be obtained based on the relation

$$\mathrm{d}_{\bar{\boldsymbol{\varepsilon}}} \bar{\boldsymbol{\sigma}}_{\mathrm{SB}} = \sum_i c^i (\,\mathrm{d}_{\boldsymbol{\varepsilon}^i} \boldsymbol{\sigma}^i)(\,\mathrm{d}_{\bar{\boldsymbol{\varepsilon}}} \boldsymbol{\varepsilon}^i). \tag{8}$$

Using $\mathrm{d}\hat{\sigma} = \partial_{\hat{\gamma}} \hat{\sigma}\; \mathrm{d}\hat{\gamma} + \partial_{\bar{\boldsymbol{\varepsilon}}} \hat{\sigma} \cdot \mathrm{d}\bar{\boldsymbol{\varepsilon}} = \hat{0}$ and

$$\boldsymbol{\varepsilon}^i = \underbrace{\bar{\boldsymbol{\varepsilon}} - \sum_j c_j \gamma_j \boldsymbol{M}_j}_{\boldsymbol{\varepsilon}_0} + \sum_{l \in \{l : r^i \cap \mathcal{SB}_l \neq \emptyset\}} \gamma_l \boldsymbol{M}_l, \tag{9}$$

$\mathrm{d}_{\bar{\boldsymbol{\varepsilon}}} \boldsymbol{\varepsilon}^i$ can easily be computed by

$$\mathbb{I}^s - \sum_j c_j \boldsymbol{M}_j \otimes (\partial_{\bar{\boldsymbol{\varepsilon}}} \gamma_j) + \sum_{l \in \{l : r^i \cap \mathcal{SB}_l \neq \emptyset\}} \boldsymbol{M}_l \otimes (\partial_{\bar{\boldsymbol{\varepsilon}}} \gamma_l). \tag{10}$$

Here, the notation introduced in [18] has been used.

6 RESULTS

In this section an elasto-plastic matrix material is used with the yield function

$$f = \|\boldsymbol{\sigma}'\| - \sqrt{\frac{2}{3}} \sigma_{\mathrm{y}}(\varepsilon^{\mathrm{eq}}), \tag{11}$$

where the equivalent plastic strain is given by

$$\dot{\varepsilon}^{\mathrm{eq}} = \sqrt{\frac{2}{3}}\|\dot{\boldsymbol{\varepsilon}}^{\mathrm{p}}\|. \tag{12}$$

Here $\boldsymbol{\sigma}'$ denotes the stress deviator and σ_{y} is the yield stress.

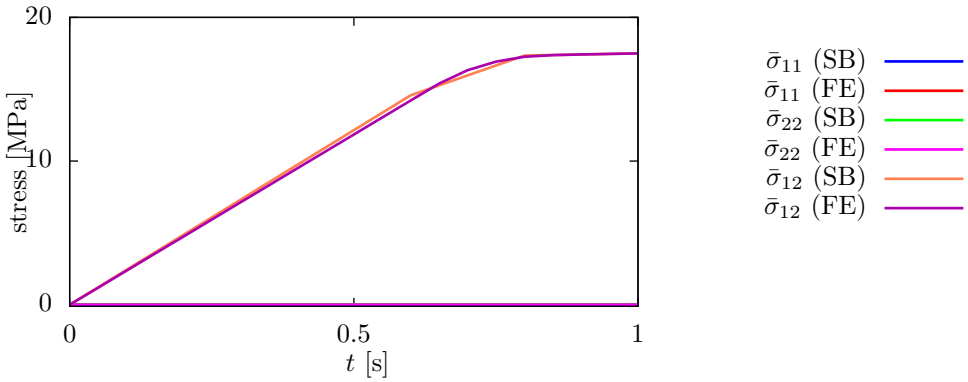

Figure 5: Comparison of FE- and shear band solution for pure shear.

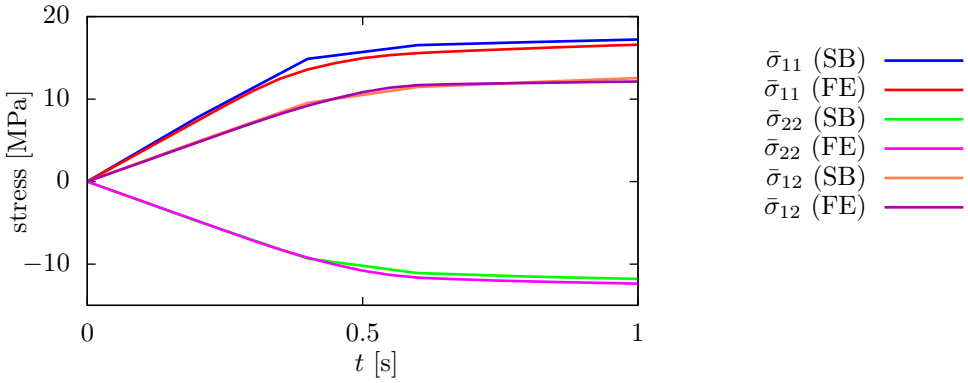

Figure 6: Comparison of FE- and shear band solution for mixed strain path.

The elasto-plastic model is applied to the matrix of the microstructure shown in Fig. 3. The inclusions (red in figure) are assumed to be isotropic and elastic. Figure 4 shows simulation results of the proposed methods in comparison with full field finite element simulations. It can be seen that the stress response of the shear band model is close to that of the finite element simulation. In addition, the predicted shear band patterns are also approximately captured by the model. The applied strain path is given by

$$\bar{\boldsymbol{\varepsilon}}(t) = \dot{\varepsilon}_0 t(\boldsymbol{e}_1 \otimes \boldsymbol{e}_1 - \boldsymbol{e}_2 \otimes \boldsymbol{e}_2). \tag{13}$$

Figure 5 shows the stress response for a prescribed macroscopic shear deformation:

$$\bar{\boldsymbol{\varepsilon}}(t) = \dot{\varepsilon}_0 t\,\mathrm{sym}(\boldsymbol{e}_1 \otimes \boldsymbol{e}_2). \tag{14}$$

Again the prediction of the stress is very close to the finite element model. The same holds for the prediction related to the following strain path

$$\bar{\boldsymbol{\varepsilon}}(t) = \dot{\varepsilon}_0 t\big(\boldsymbol{e}_1 \otimes \boldsymbol{e}_1 - \boldsymbol{e}_2 \otimes \boldsymbol{e}_2 + \mathrm{sym}(\boldsymbol{e}_1 \otimes \boldsymbol{e}_2)\big). \tag{15}$$

The related simulation results are plotted in Fig. 6. The aforementioned simulation results and material parameters are taken from [18] and are shown here only for illustration purposes.

7 SUMMARY

In this work, a fast nonlinear homogenization method for simple microstructures has been discussed which makes extensive use of shear bands. In addition, a small number of degrees of freedom and stress computations is sufficient. An example has been discussed which has been validated by FE-simulations.

ACKNOWLEDGEMENTS

Financial support of this work M03 from the Transregional Cooperative Research Center (SFB/TRR) 136 funded by the German Science Foundation (DFG) is gratefully acknowledged.

REFERENCES

[1] Dvorak, G. J. Transformation field analysis of inelastic composite materials. *Proceedings of the Royal Society of London. Series A: Mathematical and Physical Sciences 437*, 1900 (1992), 311–327.

[2] Eshelby, J. D. The determination of the elastic field of an ellipsoidal inclusion, and related problems. *Proceedings of the Royal Society of London A: Mathematical, Physical and Engineering Sciences 241*, 1226 (1957), 376–396.

[3] Feyel, F. Multiscale fe 2 elastoviscoplastic analysis of composite structures. *Computational Materials Science 16*, 1 (1999), 344–354.

[4] Fritzen, F., and Böhlke, T. Three-dimensional finite element implementation of the nonuniform transformation field analysis. *International Journal for Numerical Methods in Engineering 84*, 7 (2010), 803–829.

[5] Kochmann, J., Rezaeimianroodi, J., Reese, S., and Svendsen, B. Two-dimensional elastic phase-field simulation of fcc to bcc martensitic phase transformations in polycrystals. *PAMM 14*, 1 (2014), 397–398.

[6] Kröner, E. Berechnung der elastischen Konstanten des Vielkristalls aus den konstanten des Einkristalls. *Zeitschrift für Physik 151*, 4 (1958), 504–518.

[7] Michel, J.-C., and Suquet, P. Nonuniform transformation field analysis. *International journal of solids and structures 40*, 25 (2003), 6937–6955.

[8] Mori, T., and Tanaka, K. Average stress in matrix and average elastic energy of materials with misfitting inclusions. *Acta metallurgica 21*, 5 (1973), 571–574.

[9] Moulinec, H., and Suquet, P. A fast numerical method for computing the linear and nonlinear mechanical properties of composites. *Comptes rendus de l'Académie des sciences. Série II, Mécanique, physique, chimie, astronomie 318*, 11 (1994), 1417–1423.

[10] Reuss, A. Berechnung der Fließgrenze von Mischkristallen auf Grund der Plastizitätsbedingung für Einkristalle. *ZAMM-Journal of Applied Mathematics and Mechanics/Zeitschrift für Angewandte Mathematik und Mechanik 9*, 1 (1929), 49–58.

[11] Ryckelynck, D. Hyper-reduction of mechanical models involving internal variables. *International Journal for Numerical Methods in Engineering 77*, 1 (2009), 75–89.

[12] Shanthraj, P., Eisenlohr, P., Diehl, M., and Roters, F. Numerically robust spectral methods for crystal plasticity simulations of heterogeneous materials. *International Journal of Plasticity* (2014).

[13] Voigt, W. *Theoretische Studien über die Elasticitätsverhältnisse der Krystalle*. Königliche Gesellschaft der Wissenschaften zu Göttingen, 1887.

[14] Wulfinghoff, S., Bayerschen, E., and Böhlke, T. A gradient plasticity grain boundary yield theory. *International Journal of Plasticity 51* (2013), 33–46.

[15] Wulfinghoff, S., and Böhlke, T. Equivalent plastic strain gradient crystal plasticity – enhanced power law subroutine. *GAMM-Mitteilungen 36*, 2 (2013), 134–148.

[16] Wulfinghoff, S., and Böhlke, T. Gradient crystal plasticity including dislocation-based work-hardening and dislocation transport. *International Journal of Plasticity 69* (2015), 152–169.

[17] Wulfinghoff, S., Forest, S., and Böhlke, T. Strain gradient plasticity modeling of the cyclic behavior of laminate microstructures. *Journal of the Mechanics and Physics of Solids 79* (2015), 1–20.

[18] Wulfinghoff, S., and Reese, S. Efficient computational homogenization of simple elasto-plastic microstructures using a shear band approach. *Submitted*.